Multipole expansion for magnetic structures: A generation scheme for a symmetry-adapted orthonormal basis set in the crystallographic point group

M.-T. Suzuki,[1] T. Nomoto,[2] R. Arita,[2,3] Y. Yanagi,[1] S. Hayami,[4] and H. Kusunose[5]

[1]*Center for Computational Materials Science, Institute for Materials Research, Tohoku University, Sendai, Miyagi 980-8577, Japan*
[2]*Department of Applied Physics, University of Tokyo, 7-3-1 Hongo Bunkyo-ku, Tokyo 113-8656, Japan*
[3]*RIKEN Center for Emergent Matter Science (CEMS), Wako, Saitama 351-0198, Japan*
[4]*Department of Physics, Hokkaido University, Sapporo 060-0810, Japan*
[5]*Department of Physics, Meiji University, Kawasaki 214-8571, Japan*

We propose a systematic method to generate a complete orthonormal basis set of multipole expansion for magnetic structures in arbitrary crystal structure. The key idea is the introduction of a virtual atomic cluster of a target crystal on which we can clearly define the magnetic configurations corresponding to symmetry-adapted multipole moments. The magnetic configurations are then mapped onto the crystal so as to preserve the magnetic point group of the multipole moments, leading to the magnetic structures classified according to the irreducible representations of the crystallographic point group. We apply the present scheme to pyrochlore and hexagonal ABO$_3$ crystal structures and demonstrate that the multipole expansion is useful to investigate the macroscopic responses of antiferromagnets.

I. INTRODUCTION

Diversity of physical properties of magnets provides a fascinating playground in condensed matter physics. When we explore this exciting arena, what is interesting to note is that there are many restrictions imposed by the symmetry of the magnetic structures. For example, it has been well known that the structure of linear response tensors are determined by the magnetic point group [1–7]. Furthermore, identifying the order parameter for the magnetic phase is most useful for a deeper understanding of physical phenomena. There have been many studies to investigate the relation between the order parameters in a particular magnetic structure and macroscopic phenomena such as anomalous Hall (AH) effect [7–9], electromagnetic (EM) effect [10–15], and optical responses [16]. Thus we have a significant chance to specify or even design a magnet exhibiting desired physical properties by investigating the order parameters which characterize the magnetic structures.

For this purpose, the multipole expansion of the magnetic structure is an efficient and powerful approach. Indeed, the multipole moments inherent in the magnetic structure, which we call cluster multipole moments [7], have played a crucial role as a key order parameter in a variety of studies: EM effect has been discussed in terms of the magnetic (M), rank-0 monopole, and rank-2 quadrupole as well as the magnetic toroidal (MT) rank-1 dipole as the order parameter to

characterize the specific magnetic structures [10–12,17]. The relation between parity odd multipoles and electromagnetic effect has recently been investigated based on generalized forms of the multipole expansions for magnetic distributions [14,15]. It has also been shown that the rank-3 M multipole (octupole) plays a key role for a large AH effect [18–20], anomalous Nernst effect [21], and magneto-optical Kerr effect [16] in the coplanar antiferromagnets Mn$_3Z$ (Z = Sn, Ge) [7]. In these studies, the interplay between the physical properties and the magnetic structure through cluster multipoles has been investigated extensively. However, there has been no concrete scheme to make a complete basis set of cluster multipoles for a given crystal structure.

In this paper, we propose a scheme to generate cluster multipoles which form a complete orthonormal basis set for arbitrary magnetic structures. Here, we introduce a virtual atomic cluster which depends only on the crystallographic point group of the system. We define unambiguously the magnetic configurations corresponding to the symmetry-adapted multipoles in the atomic cluster. The obtained magnetic configurations are mapped to the original crystal structure with the magnetic point-group symmetry preserved. The generated complete basis set for the magnetic structure in crystal is useful to measure the symmetry breaking as an order parameter according to the magnetic point group [7]. Although we restrict ourselves to the case with "uniform" magnetic structures characterized by the ordering vector $\boldsymbol{q} = 0$ in this paper, an extension to cases with nonzero $\boldsymbol{q}$ ordering vectors is straightforward.

To demonstrate the efficiency of the present scheme, we apply the cluster multipole expansion of magnetic structures to pyrochlore and hexagonal ABO$_3$ crystal structures. For the pyrochlore structure, it is shown that the all-in all-out

magnetic structure corresponds to a M octupole, and two-in two-out and one-in three-out magnetic structures are expressed by the linear combinations of the M dipole and octupole that belong to the same irreducible representation (IREP) of the crystallographic point group. The two-in two-out and one-in three-out magnetic structures can be transformed continuously to the pure antiferromagnetic structures, indicating that the antiferromagnetic structures without net magnetization yield the AH effect. For the hexagonal ABO_3 structure, higher-rank multipoles such as MT quadrupole and M octupole are necessary to describe the magnetic structures exhibiting the AH and EM effects within the uniform magnetic ordering.

II. MULTIPOLE EXPANSION OF MAGNETIC STRUCTURES IN CRYSTAL

A. Outline of multipole expansion of magnetic structures in crystal

In this paper, we present a method to generate an orthonormal complete basis set of magnetic structures corresponding to the cluster multipoles classified according to the IREPs of the crystallographic point group. To eliminate confusion and ambiguity, we define some words used in this paper. "Atomic cluster" is used for the atoms transformed to each other only by the rotation operations of a point group and is distinguished from "crystal," which assumes a periodicity for an atomic configuration. "Magnetic configuration" is used for the alignment of magnetic dipole moments on atoms of the atomic cluster and is distinguished from "magnetic structure," which is for the alignment of magnetic dipole moments on atoms in periodic crystal. A magnetic configuration (a magnetic structure) characterized by M and/or MT multipoles is called a multipole magnetic configuration (multipole magnetic structure). The outline of the generation procedure for the orthonormal multipole magnetic structures in crystal is as follows (see also Fig. 1):

(1) Set a virtual atomic cluster corresponding to the crystallographic point group of a target crystal.

(2) Generate magnetic configurations corresponding to the symmetrized M and MT multipoles in the virtual atomic cluster.

(3) Map the magnetic dipole moments on the atoms in the virtual atomic cluster to those on the crystallographically equivalent atoms in crystal, which represent the multipole magnetic structures.

(4) Orthonormalize the bases of multipole magnetic structures by using the Gram-Schmidt orthogonalization procedure.

Details for the procedure are explained in Secs. II C, II D, and II E. With this method, all the generated orthonormal magnetic structures are characterized by the symmetry-adapted multipoles. Thus, the multipoles can be a useful measure of symmetry breaking of the crystallographic point group in the presence of the uniform magnetic orders. It is a natural extension of conventional dipole magnetization which measures the symmetry breaking of the ferromagnetic order. The multipole expansion for magnetic structures in crystal is very efficient to investigate the relation between the magnetic structures and physical properties beyond the symmetry analysis.

B. Multipole magnetic configurations in atomic clusters

The multipole expansion of the vector gauge potential is given under the Coulomb gauge $\nabla \cdot A(r) = 0$ as follows:

$$A(r) = \sum_{\ell m}\left(b_\ell M_{\ell m} \frac{Y_{\ell m}^\ell(\hat{r})}{r^{\ell+1}} + c_\ell T_{\ell m} \frac{Y_{\ell m}^{\ell+1}(\hat{r})}{r^{\ell+2}} \right), \qquad (1)$$

where $Y_{\ell m}^{\ell'}(\hat{r})$ ($\ell \geqslant 1$, $-\ell \leqslant m \leqslant \ell$, $\ell' = \ell - 1, \ell, \ell + 1$) is the vector spherical harmonics that transforms as conventional scalar spherical harmonics $Y_{\ell m}(\hat{r})$ for rotation operation with its orbital angular momentum ℓ' [22–24]. The expansion coefficients in Eq. (1) are the so-called M multipole, $M_{\ell m}$, and MT multipole, $T_{\ell m}$, respectively (b_ℓ and c_ℓ are introduced for convenience). The M and MT multipoles around a single
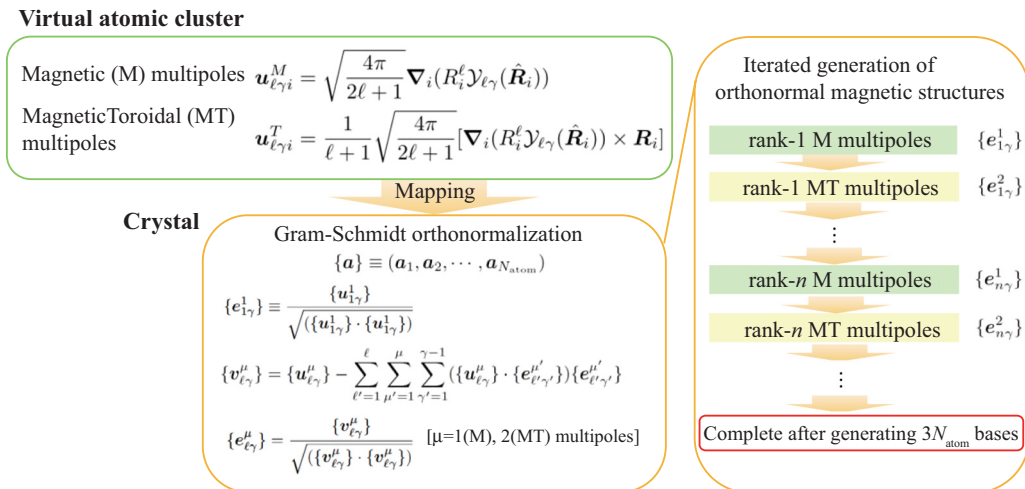

FIG. 1. Outline of the generation procedure for a $3N_{\text{atom}}$ complete basis set of multipole magnetic structure classified by the crystallographic point group.

magnetic ion in the unit of Bohr magneton are defined as

$$M_{\ell m} = \sum_j \left(\frac{2\boldsymbol{\ell}_j}{\ell+1} + \boldsymbol{\sigma}_j \right) \cdot \boldsymbol{O}_{lm}(\boldsymbol{r}_j), \qquad (2)$$

$$T_{\ell m} = \sum_j \left\{ \frac{\boldsymbol{r}_j}{\ell+1} \times \left(\frac{2\boldsymbol{\ell}_j}{\ell+2} + \boldsymbol{\sigma}_j \right) \right\} \cdot \boldsymbol{O}_{lm}(\boldsymbol{r}_j), \qquad (3)$$

with

$$\boldsymbol{O}_{lm}(\boldsymbol{r}) \equiv \sqrt{\frac{4\pi}{2\ell+1}} \nabla[r^\ell Y_{\ell m}^*(\hat{\boldsymbol{r}})], \qquad (4)$$

where $\boldsymbol{\ell}_j$ and $\boldsymbol{\sigma}_j$ are the orbital and spin angular momentum of an electron at $\boldsymbol{r}_j$. Here, $r = |\boldsymbol{r}|$ and $\hat{\boldsymbol{r}} = \boldsymbol{r}/r$. Since the vector spherical harmonics $\boldsymbol{Y}_{\ell m}^{\ell'}$ are an orthonormal complete basis set of a vector function on a sphere, the M and MT multipoles $M_{\ell m}$ and $T_{\ell m}$ represent the arbitrary angular dependence of the magnetization distribution on a single magnetic ion. Focusing on the spin part of Eqs. (2) and (3), the M and MT multipoles can be extended straightforwardly to characterize the classical magnetic configurations $\{\boldsymbol{m}_i\}$ in an atomic cluster whose atoms are transformed to each other through the point-group symmetry operations with respect to the symmetry center of the atomic cluster. The explicit definitions are given as

$$M_{\ell m} \equiv \sum_{i=1}^{N_{\text{atom}}} \boldsymbol{m}_i \cdot \boldsymbol{O}_{lm}(\boldsymbol{R}_i), \qquad (5)$$

$$T_{\ell m} \equiv \frac{1}{\ell+1} \sum_{i=1}^{N_{\text{atom}}} (\boldsymbol{R}_i \times \boldsymbol{m}_i) \cdot \boldsymbol{O}_{lm}(\boldsymbol{R}_i), \qquad (6)$$

where $\boldsymbol{R}_i$ is the position vector of ith atom, and N_{atom} is the number of atoms in the atomic cluster. These multipoles transform in the same manner as the spherical harmonics $Y_{\ell m}$ for rotation operation of the point group with the odd parity for the time-reversal operation, and hence they are classified according to the IREPs of the point group [14]. The spherical harmonics are usually symmetrized according to the IREPs as

$$\mathcal{Y}_{\ell\gamma}(\hat{\boldsymbol{r}}) = \sum_m c_{\ell m}^\gamma Y_{\ell m}(\hat{\boldsymbol{r}}), \qquad (7)$$

where γ runs from 1 to $2\ell+1$ in order to distinguish the IREP and its component, including multiplicity, which is necessary when the same IREPs multiply appear in the same rank ℓ. The coefficients $c_{\ell m}^\gamma$ of the symmetrized spherical harmonics $\mathcal{Y}_{\ell\gamma}(\hat{\boldsymbol{r}})$ are tabulated in Ref. [23], for instance, where $c_{\ell m}^\gamma$ are chosen so that $\mathcal{Y}_{\ell\gamma}(\hat{\boldsymbol{r}})$ is real. This is always possible in the presence of the time-reversal symmetry. The symmetry-adapted multipoles are thus reexpressed as follows:

$$M_{\ell\gamma} = \sum_{i=1}^{N_{\text{atom}}} \boldsymbol{u}_{\ell\gamma i}^M \cdot \boldsymbol{m}_i, \qquad (8)$$

$$T_{\ell\gamma} = \sum_{i=1}^{N_{\text{atom}}} \boldsymbol{u}_{\ell\gamma i}^T \cdot \boldsymbol{m}_i, \qquad (9)$$

where

$$\boldsymbol{u}_{\ell\gamma i}^M = \boldsymbol{\mathcal{O}}_{l\gamma}(\boldsymbol{R}_i), \qquad (10)$$

$$\boldsymbol{u}_{\ell\gamma i}^T = \frac{1}{\ell+1}(\boldsymbol{\mathcal{O}}_{l\gamma}(\boldsymbol{R}_i) \times \boldsymbol{R}_i), \qquad (11)$$

and $\boldsymbol{\mathcal{O}}_{l\gamma}$ is given by replacing Y_{lm}^* in Eq. (4) with $\mathcal{Y}_{l\gamma}$. The cluster multipole order parameter, defined in Eq. (10) or (11), is a natural generalization of the magnetization in FM states, including the magnetization as the rank-1 M multipole in Eq. (10).

In generating an orthogonal basis set of the magnetic structures based on the symmetry, the conventional projection operator method requires nontrivial trials to find out the suitable trial functions and becomes complicated when the crystal contains many magnetic atoms. Moreover, that procedure has large ambiguity for low-symmetry crystals, and for the complicated magnetic structures, it would be difficult to find out the correspondence between the magnetic structures and symmetry-adapted multipoles. On the contrary, our method is highly advantageous, since it is possible to automatically generate a complete orthonormal basis set of magnetic structures, and it is, by definition, based on the symmetry-adapted multipoles

Here, we comment on the so-called M monopole or magnetic flux configuration that corresponds to a magnetic configuration in which all the magnetic dipole moments point to the center of the atomic cluster. The monopole magnetic configuration is parity odd and invariant under all the rotational symmetry operations of the point group. Such a monopole magnetic configuration can be defined as [12,17]

$$\boldsymbol{u}_{01i}^M \equiv \frac{\boldsymbol{R}_i}{R_i^2}. \qquad (12)$$

In this paper, however, we do not include this type of M monopole in the cluster multipole expansion, since the ordinary multipole expansion in Eq. (1) does not contain the monopole term, and the corresponding magnetic configuration always appears as a higher-rank multipole of the parity odd fully symmetric IREP, as will be shown in the case of hexagonal ABO_3 in Sec. III C.

C. Virtual atomic clusters for crystallographic point groups

In crystal, crystallographically equivalent atoms are transformed to each other by combinations of point-group symmetry operation $\mathcal{R}_i$, nonprimitive translation $\boldsymbol{\tau}_j$, and primitive translation $\boldsymbol{T}_j$, which constitute the symmetry operations of the space group. According to Neumann's principle, the appearance of macroscopic phenomena such as AH and EM effects are determined by the crystallographic point group, whose symmetry operations consist only of the rotation part $\mathcal{R}_i$ of the space group. Therefore, in order to discuss the macroscopic phenomena induced by the antiferromagnetic order, it is necessary to define appropriate order parameters for antiferromagnetic order reflecting the symmetry breaking of the crystallographic point group.

The crystallographic point group corresponding to the space group of crystal is more definitely defined as follows. The space group $\mathcal{G}$ is decomposed as

$$\mathcal{G} = \sum_{i=1}^{N_{\text{coset}}} \{\mathcal{R}_i|\boldsymbol{\tau}_i\}\mathcal{H}T, \qquad (13)$$

where the subgroup $\mathcal{H}$ consists only of the pure rotation symmetry operations $\{h_1, h_2, \ldots, h_{N_0}\}$, T is the group consisting

of lattice translations $\boldsymbol{T}_j$, and $\{\mathcal{R}_i|\boldsymbol{\tau}_i\}$ are representative elements of $\mathcal{G}$ with rotation operation $\mathcal{R}_i$ [$\mathcal{R}_1 = E$ (identity operation)] and nonprimitive translation operation $\boldsymbol{\tau}_i$ ($\boldsymbol{\tau}_1 = \boldsymbol{0}$). N_{coset} is the number of cosets. Note that the terms with $i \geqslant 2$ in Eq. (13) exist only in nonsymmorphic space groups. The crystallographic point group $\mathcal{P}$ corresponding to the space group $\mathcal{G}$ is then defined as

$$\mathcal{P} = \sum_{i=1}^{N_{\text{coset}}} \{\mathcal{R}_i|\boldsymbol{0}\}\mathcal{H}. \tag{14}$$

Magnetic configurations in an atomic cluster are unambiguously defined by multipoles through Eqs. (8) and (9). This is in high contrast to a direct generation of magnetic structures in crystal, which is not straightforward since the atoms in crystal are related not only by rotation operations but also by translation operations, as we discussed in Ref. [7]. To avoid difficulties in the direct generation of magnetic structures in crystal, our strategy to generate the symmetry-adapted magnetic structures in crystal is to generate the multipole magnetic configurations at first in a virtual atomic cluster defined under the point group $\mathcal{P}$ and then map the magnetic configurations onto the magnetic structure in crystal so as to preserve the magnetic point-group symmetry of the multipole configurations. The virtual atomic cluster is defined as an atomic cluster consisting of the same number of atoms as the symmetry operations in the crystallographic point group $\mathcal{P}$, in which their atomic positions are given as the general Wyckoff

positions of the corresponding symmorphic space group, as listed in Table I for representative point groups. In the virtual atomic cluster, the magnetic configurations corresponding to the M and MT multipoles, Eqs. (8) and (9), are obtained by Eqs. (10) and (11), respectively, with respect to the origin of the virtual atomic cluster. The examples of the virtual atomic clusters are depicted in Fig. 2 for the O_h, C_{4h}, D_{6h}, C_{6v} point groups. Note that the virtual atomic cluster has ambiguity due to the choice of the parameter x, y, z, as seen in Table I. This leads to an arbitrariness of the magnetic configurations in the virtual atomic cluster. This arbitrariness is largely reduced when the magnetic configuration is mapped onto the atoms at high-symmetry sites in crystal, as explained in Sec. II D.

D. Mapping of multipoles from virtual atomic cluster to crystal

The purpose of this section is to obtain the magnetic structures whose transformation property for the magnetic point-group operations is the same with that of multipole configurations in the virtual atomic cluster. For this purpose, we first choose one atom in the virtual atomic cluster and one in crystal and set the same M dipole moments on these atoms by setting a mapping from the atoms in the virtual atomic cluster to that in crystal. The whole mapping between the atoms in the virtual atomic cluster and the symmetrically equivalent atoms in crystal is obtained by identifying the atoms transformed by the point-group symmetry operations R_i in the virtual atomic cluster with the atoms transformed by

TABLE I. List of atomic positions of virtual atomic clusters for representative crystallographic point groups. Those for other point groups are found in Ref. [25] as general Wyckoff positions of symmorphic space groups as well as the listed point groups.

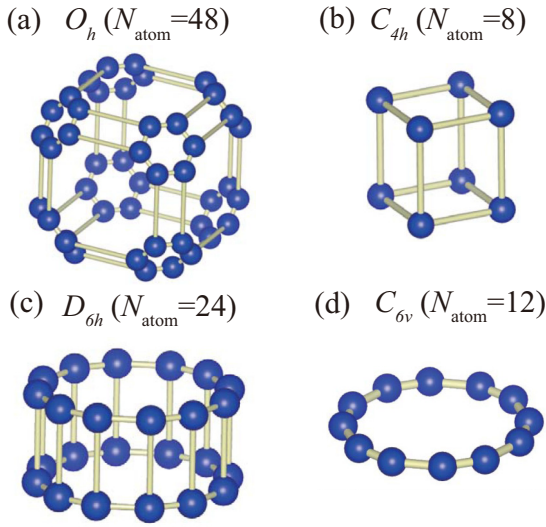|	Atomic positions of virtual atomic clusters
O_h	(1) x, y, z (2) $\bar{x}, \bar{y}, z$ (3) $\bar{x}, y, \bar{z}$ (4) $x, \bar{y}, \bar{z}$ (5) z, x, y (6) $z, \bar{x}, \bar{y}$ (7) $\bar{z}, \bar{x}, y$ (8) $\bar{z}, x, \bar{y}$
	(9) y, z, x (10) $\bar{y}, z, \bar{x}$ (11) $y, \bar{z}, \bar{x}$ (12) $\bar{y}, \bar{z}, x$ (13) $y, x, \bar{z}$ (14) $\bar{y}, \bar{x}, \bar{z}$ (15) $y, \bar{x}, z$ (16) $\bar{y}, x, z$
	(17) $x, z, \bar{y}$ (18) $\bar{x}, z, y$ (19) $\bar{x}, \bar{z}, \bar{y}$ (20) $x, \bar{z}, y$ (21) $z, y, \bar{x}$ (22) $z, \bar{y}, x$ (23) $\bar{z}, y, x$ (24) $\bar{z}, \bar{y}, \bar{x}$
	(25) $\bar{x}, \bar{y}, \bar{z}$ (26) $x, y, \bar{z}$ (27) $x, \bar{y}, z$ (28) $\bar{x}, y, z$ (29) $\bar{z}, \bar{x}, \bar{y}$ (30) $\bar{z}, x, y$ (31) $z, x, \bar{y}$ (32) $z, \bar{x}, y$
	(33) $\bar{y}, \bar{z}, \bar{x}$ (34) $y, \bar{z}, x$ (35) $\bar{y}, z, x$ (36) $y, z, \bar{x}$ (37) $\bar{y}, \bar{x}, z$ (38) y, x, z (39) $\bar{y}, x, \bar{z}$ (40) $y, \bar{x}, \bar{z}$
	(41) $\bar{x}, \bar{z}, y$ (42) $x, \bar{z}, \bar{y}$ (43) x, z, y (44) $\bar{x}, z, \bar{y}$ (45) $\bar{z}, \bar{y}, x$ (46) $\bar{z}, y, \bar{x}$ (47) $z, \bar{y}, \bar{x}$ (48) z, y, x
O	(1) x, y, z (2) $\bar{x}, \bar{y}, z$ (3) $\bar{x}, y, \bar{z}$ (4) $x, \bar{y}, \bar{z}$ (5) z, x, y (6) $z, \bar{x}, \bar{y}$ (7) $\bar{z}, \bar{x}, y$ (8) $\bar{z}, x, \bar{y}$
	(9) y, z, x (10) $\bar{y}, z, \bar{x}$ (11) $y, \bar{z}, \bar{x}$ (12) $\bar{y}, \bar{z}, x$ (13) $y, x, \bar{z}$ (14) $\bar{y}, \bar{x}, \bar{z}$ (15) $y, \bar{x}, z$ (16) $\bar{y}, x, z$
	(17) $x, z, \bar{y}$ (18) $\bar{x}, z, y$ (19) $\bar{x}, \bar{z}, \bar{y}$ (20) $x, \bar{z}, y$ (21) $z, y, \bar{x}$ (22) $z, \bar{y}, x$ (23) $\bar{z}, y, x$ (24) $\bar{z}, \bar{y}, \bar{x}$
T_d	(1) x, y, z (2) $\bar{x}, \bar{y}, z$ (3) $\bar{x}, y, \bar{z}$ (4) $x, \bar{y}, \bar{z}$ (5) z, x, y (6) $z, \bar{x}, \bar{y}$ (7) $\bar{z}, \bar{x}, y$ (8) $\bar{z}, x, \bar{y}$
	(9) y, z, x (10) $\bar{y}, z, \bar{x}$ (11) $y, \bar{z}, \bar{x}$ (12) $\bar{y}, \bar{z}, x$ (13) y, x, z (14) $\bar{y}, \bar{x}, z$ (15) $y, \bar{x}, \bar{z}$ (16) $\bar{y}, x, \bar{z}$
	(17) x, z, y (18) $\bar{x}, z, \bar{y}$ (19) $\bar{x}, \bar{z}, y$ (20) $x, \bar{z}, \bar{y}$ (21) z, y, x (22) $z, \bar{y}, \bar{x}$ (23) $\bar{z}, y, \bar{x}$ (24) $\bar{z}, \bar{y}, x$
T_h	(1) x, y, z (2) $\bar{x}, \bar{y}, z$ (3) $\bar{x}, y, \bar{z}$ (4) $x, \bar{y}, \bar{z}$ (5) z, x, y (6) $z, \bar{x}, \bar{y}$ (7) $\bar{z}, \bar{x}, y$ (8) $\bar{z}, x, \bar{y}$
	(9) y, z, x (10) $\bar{y}, z, \bar{x}$ (11) $y, \bar{z}, \bar{x}$ (12) $\bar{y}, \bar{z}, x$ (13) $\bar{x}, \bar{y}, \bar{z}$ (14) $x, y, \bar{z}$ (15) $x, \bar{y}, z$ (16) $\bar{x}, y, z$
	(17) $\bar{z}, \bar{x}, \bar{y}$ (18) $\bar{z}, x, y$ (19) $z, x, \bar{y}$ (20) $z, \bar{x}, y$ (21) $\bar{y}, \bar{z}, \bar{x}$ (22) $y, \bar{z}, x$ (23) $\bar{y}, z, x$ (24) $y, z, \bar{x}$
C_{4h}	(1) x, y, z (2) $\bar{x}, \bar{y}, z$ (3) $\bar{y}, x, z$ (4) $y, \bar{x}, z$ (5) $\bar{x}, \bar{y}, \bar{z}$ (6) $x, y, \bar{z}$ (7) $y, \bar{x}, \bar{z}$ (8) $\bar{y}, x, \bar{z}$
D_{6h}	(1) x, y, z (2) $\bar{y}, x - y, z$ (3) $\bar{x} + y, \bar{x}, z$ (4) $\bar{x}, \bar{y}, z$ (5) $y, \bar{x} + y, z$ (6) $x - y, x, z$ (7) $y, x, \bar{z}$ (8) $x - y, \bar{y}, \bar{z}$
	(9) $\bar{x}, \bar{x} + y, \bar{z}$ (10) $\bar{y}, \bar{x}, \bar{z}$ (11) $\bar{x} + y, y, \bar{z}$ (12) $x, x - y, \bar{z}$ (13) $\bar{x}, \bar{y}, \bar{z}$ (14) $y, \bar{x} + y, \bar{z}$ (15) $x - y, x, \bar{z}$ (16) $x, y, \bar{z}$
	(17) $\bar{y}, z - y, \bar{z}$ (18) $\bar{x} + y, x, \bar{z}$ (19) $\bar{y}, \bar{x}, z$ (20) $\bar{x} + y, y, z$ (21) $x, x - y, z$ (22) y, x, z (23) $x - y, \bar{y}, z$ (24) $\bar{x}, \bar{x} + y, z$
C_{6v}	(1) x, y, z (2) $\bar{y}, x - y, z$ (3) $\bar{x} + y, \bar{x}, z$ (4) $\bar{x}, \bar{y}, z$ (5) $y, \bar{x} + y, z$ (6) $x - y, x, z$ (7) $\bar{y}, \bar{x}, z$ (8) $\bar{x} + y, y, z$,
	(9) $x, x - y, z$ (10) y, x, z (11) $x - y, \bar{y}, z$ (12) $\bar{x}, \bar{x} + y, z$
D_{3d}	(1) x, y, z (2) $\bar{y}, x - y, z$ (3) $\bar{x} + y, \bar{x}, z$ (4) $\bar{y}, \bar{x}, \bar{z}$ (5) $\bar{x} + y, y, \bar{z}$ (6) $x, x - y, \bar{z}$ (7) $\bar{x}, \bar{y}, \bar{z}$ (8) $y, \bar{x} + y, \bar{z}$
	(9) $x - y, x, \bar{z}$ (10) y, x, z (11) $x - y, \bar{y}, z$ (12) $\bar{x}, \bar{x} + y, z$

(a) O_h (N_{atom}=48) (b) C_{4h} (N_{atom}=8)

(c) D_{6h} (N_{atom}=24) (d) C_{6v} (N_{atom}=12)

FIG. 2. Examples of virtual atomic clusters for (a) O_h, (b) C_{4h}, (c) D_{6h}, and (d) C_{6v} point groups.

the symmetry operations of the space group, $\{E|\boldsymbol{T}_j\}\{R_i|\boldsymbol{\tau}_i\}h_k$, in the crystal for the initially chosen atoms in both systems. The mapping from the atoms in the virtual atomic cluster to the symmetrically equivalent atoms in crystal obviously does not have one-to-one correspondence.

The M dipole moment on an atom in crystal is obtained by summing up the M dipole moments on all of the corresponding atoms in the virtual atomic cluster, as will be discussed in Sec. III A. The generated magnetic structures in crystal are fully characterized by the symmetry-adapted multipoles in the virtual atomic cluster through the mapping, which we call the multipole magnetic structures. We note that the correspondence between generated magnetic structures and multipole configurations depends on the choice of the first mapping between the atoms in the virtual atomic cluster and that in crystal. It occurs especially for low-symmetry crystallographic point groups having the multiple symmetrized bases within the same IREPs and rank. In this case, we have to specify the representative atoms in the virtual atomic cluster and in crystal to identify the correspondence between the magnetic structures and multipole configurations. The other arbitrariness for the multipole structures arises from the choice of parameters (x, y, z) of the virtual atomic cluster as listed in Table I, as already mentioned in Sec. II C.

The advantage to introducing the virtual atomic cluster is that once we generate the multipole magnetic configurations in the virtual atomic cluster, we can systematically generate complete orthonormal basis sets for arbitrary crystal structures by appropriate mappings in which they share a common point group between the atomic cluster and the crystal. This is in high contrast with our previous scheme proposed in Ref. [7] to identify the multipoles in crystal. In the previous scheme, the atomic cluster is defined not in a virtual one but directly for the atoms in the crystal. We identified N_{coset} clusters in which one consists of the atoms transformed to each other by the point-group operations of $\mathcal{H}$ in Eq. (13) and the others are determined from transformation of $\{\mathcal{R}_i|\boldsymbol{\tau}_i\}\mathcal{H}$ for the cluster in the crystal unit cell. The macroscopic multipole

moment was obtained by summing up the multipole moments in each cluster in accordance with a nonsymmorphic space group of Mn_3Z (Z = Sn, Ge). However, there are some cases that the higher-rank multipoles are ill defined, especially when the magnetic atoms are located at high-symmetry sites. The present scheme does not cause this problem and is advantageous in its efficiency, since the arbitrariness of the generated orthonormal magnetic structures is largely reduced as compared with the conventional method using a projection operator [26,27], whose generated magnetic structures highly depend on the choice of the trial functions to be operated. Based on the present procedure, we can systematically and automatically generate magnetic structures corresponding to the multipoles according to the IREPs of the crystallographic point group of the focusing crystal.

E. Orthonormalization of basis set for magnetic structure in crystal

The multipole expansion in Eq. (1) requires an infinite number of components to express magnetization distribution in continuous space. In contrast, the multipole expansion in magnetic structures that does not break the crystal periodicity is represented by a linear combination of a $3N_{atom}$ orthogonal basis set, where N_{atom} is the number of atoms in a crystal unit cell. In this section, we explain how to obtain the $3N_{atom}$ orthonormal basis set which is sufficient to express a uniform magnetic order.

For notational convenience, we introduce the vector notation for uniform magnetic structures $\{\boldsymbol{a}\} = (\boldsymbol{a}_1, \boldsymbol{a}_2, \ldots, \boldsymbol{a}_{N_{atom}})$, where $\boldsymbol{a}_i$ represents the three-component vector on the ith atom in the crystal unit cell. Usually, the magnetic structure $\{\boldsymbol{m}_i\}$ is decomposed into the ferromagnetic part $\{\boldsymbol{m}_i^{FM}\}$, where $\boldsymbol{m}_i^{FM} = \sum_i \boldsymbol{m}_i / N_{atom}$, and the residual antiferromagnetic part $\{\boldsymbol{m}_i^{AFM}\}$, where $\boldsymbol{m}_i^{AFM} = \boldsymbol{m}_i - \boldsymbol{m}_i^{FM}$ [10]. Such a decomposition for the magnetic structure is generalized to obtain the $3N_{atom}$ orthonormal complete basis set by using Gram-Schmidt orthonormalization procedure as follows:

$$\{\boldsymbol{e}_{1\gamma}^1\} \equiv \frac{\{\boldsymbol{u}_{1\gamma}^1\}}{\sqrt{(\{\boldsymbol{u}_{1\gamma}^1\} \cdot \{\boldsymbol{u}_{1\gamma}^1\})}}, \tag{15}$$

$$\{\boldsymbol{v}_{\ell\gamma}^\mu\} = \{\boldsymbol{u}_{\ell\gamma}^\mu\} - \sum_{\ell'=1}^{\ell} \sum_{\mu'=1}^{\mu} \sum_{\gamma'=1}^{\gamma-1} (\{\boldsymbol{u}_{\ell\gamma}^\mu\} \cdot \{\boldsymbol{e}_{\ell'\gamma'}^{\mu'}\}) \{\boldsymbol{e}_{\ell'\gamma'}^{\mu'}\}, \tag{16}$$

$$\{\boldsymbol{e}_{\ell\gamma}^\mu\} = \frac{\{\boldsymbol{v}_{\ell\gamma}^\mu\}}{\sqrt{(\{\boldsymbol{v}_{\ell\gamma}^\mu\} \cdot \{\boldsymbol{v}_{\ell\gamma}^\mu\})}}, \tag{17}$$

where $\mu = 1$ and 2 represents the M and MT multipoles, respectively. The initial $\boldsymbol{u}_{1\gamma}^1$ in Eq. (15) is set as the M dipole moments M_x, M_y, and M_z for $\gamma = 1, 2, 3$, respectively. The iterated calculation of the Gram-Schmidt orthonormalization procedure, Eqs. (16) and (17), starting from the lower-rank multipoles to higher ones as shown in Fig. 1, automatically generates an orthonormal complete basis set of the uniform magnetic structures classified according to the IREPs of the crystallographic point group. After the orthonormalization procedure, the magnetic structures corresponding to the

higher-rank multipole may not be the pure multipole with definite rank as in Eq. (16). However, since the subtraction in Eq. (16) is to eliminate the overlap between the highest-rank multipole and the lower ones, and $\{e^\mu_{\ell\gamma}\}$ in Eq. (17) always contains $\{u^\mu_{\ell\gamma}\}$, it can be regarded as the rank-ℓ multipole.

The generated finite norm of vectors $\{e^\mu_{\ell\gamma}\}$ are stored sequentially as $\{e^i\}$ with the sequential indices $i = 1, ..., 3N_{\text{atom}}$. With this procedure, the ferromagnetic structures $\{e^i\}$ with $i \leqslant 3$ are orthogonal to the antiferromagnetic structures with $i > 3$. The obtained magnetic structure basis sets are orthonormal, i.e., $(\{e^i\} \cdot \{e^j\}) = \delta_{ij}$. Since the obtained basis set is complete for the uniform magnetic structures, the arbitrary uniform magnetic structure can be expressed as $\{m\} = \sum_{i=1}^{3N_{\text{atom}}} c_i\{e^i\}$, with $c_i = (\{m\} \cdot \{e^i\})$. Note that the relation $\sum_i^{3N_{\text{atom}}} |c_i|^2 = \sum_i^{N_{\text{atom}}} |m_i|^2$ holds.

III. EXAMPLES OF MULTIPOLE EXPANSION FOR CRYSTALS

A. Simple examples

Here we illustrate the correspondence between the symmetry-adapted multipole magnetic configurations in the virtual atomic cluster and magnetic structures in crystal. We take two simple examples, i.e., the atoms placed at $8l$ and $2e$ Wyckoff sites in symmorphic space group $P4/m$ (No. 83), and $8k$ and $2a$ Wyckoff sites in nonsymmorphic space group $P4_2/m$ (No. 84). The crystallographic point group of both space groups is C_{4h}, which corresponds to a virtual atomic cluster consisting of eight atoms transformed to each other through the symmetry operations, as shown in Fig. 2(b). In Fig. 3, twofold rotation C_2 transforms atom 1 to atom 2, fourfold rotation C_4 to atom 3, C_4^{-1} to atom 4, space inversion I to atom 5, IC_2 to atom 6, IC_4 to atom 7, and IC_4^{-1} to atom 8. These transformation relations provide mapping from the atoms in the virtual atomic cluster to symmetrically equivalent atoms in the crystal as discussed in Sec. II D. Figures 3 and 4 show the relation between the atoms in the virtual atomic cluster and the atoms at the Wyckoff sites in crystal.
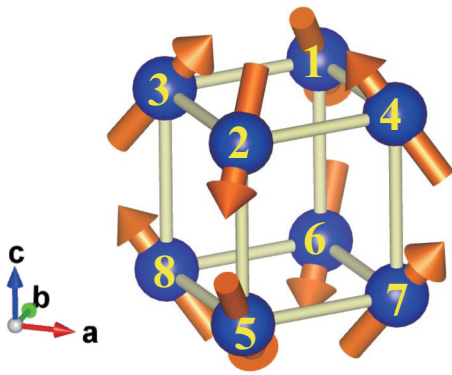
FIG. 3. Magnetic configuration of the MT quadrupole in B_g IREP of the C_{4h} point group in the virtual atomic cluster, placing an atom labeled 1 at $(0,0.3,0.3)$, which is obtained by Eq. (11) with $\mathcal{Y}_{25}$ in Eq. (18).
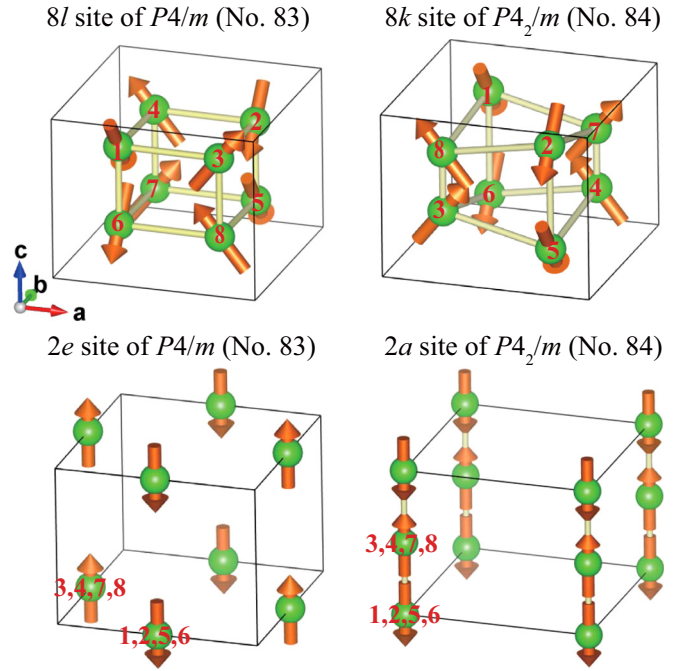
FIG. 4. MT quadrupoles in crystals belonging to the $P4/m$ and $P4_2/m$ space groups, which are obtained by mapping from the C_{4h} virtual atomic cluster as shown in Fig. 3.

For the C_{4h} point group, the rank-2 spherical harmonics are symmetrized as

$$
\begin{aligned}
\mathcal{Y}_{21} &= Y_{20} \quad (A_g), \\
\mathcal{Y}_{22} &= \frac{1}{\sqrt{2}}(Y_{2-1} - Y_{21}) \quad (E_g), \\
\mathcal{Y}_{23} &= \frac{1}{\sqrt{2}i}(Y_{2-1} + Y_{21}) \quad (E_g), \\
\mathcal{Y}_{24} &= \frac{1}{\sqrt{2}}(Y_{2-2} + Y_{22}) \quad (B_g), \\
\mathcal{Y}_{25} &= \frac{1}{\sqrt{2}i}(Y_{2-2} - Y_{22}) \quad (B_g).
\end{aligned}
\tag{18}
$$

The multipole configurations are calculated from Eqs. (10) and (11) on the virtual atomic cluster as shown in Fig. 2(b), where atom 1 is placed at (0, 0.3, 0,3). Figure 3 shows the magnetic configuration generated from Eq. (11) with the symmetrized spherical harmonics $\mathcal{Y}_{25}$ in Eq. (18), corresponding to the MT quadrupole T_{xy}, classified to B_g IREP of the C_{4h} point group [14]. This magnetic configuration in the virtual atomic cluster is mapped to symmetrically equivalent atoms, denoted by the signatures of Wyckoff positions, to obtain the corresponding magnetic structures in crystals as shown in Fig. 4. For the general Wyckoff positions in each crystal ($8l$ site of $P4/m$ and $8k$ site of $P4_2/m$), the magnetic structures are straightforwardly obtained through the mapping (Fig. 4). Meanwhile, for the $2e$ site of $P4/m$ and $2a$ site of $P4_2/m$, multiple atoms in the virtual cluster are mapped to the same atoms in the crystal, leading to the cancellation of the M dipole moment that is consistent with the symmetry in these Wyckoff sites.

TABLE II. Relation between the multipoles corresponding to the orthonormal magnetic structures for pyrochlore crystal structure and IREP for the crystallographic point group O_h, as well as the magnetic point group with its principal axis. The active component of the AH conductivity (AHC) is also shown.

No.	IREP	Multipole	MPG	P. axis	AHC
1	T_{1g}	M_x	$4/mm'm'$	[100]	σ_{yz}
2		M_y	$4/mm'm'$	[010]	σ_{zx}
3		M_z	$4/mm'm'$	[001]	σ_{xy}
4	E_g	T_v	$4/mmm$	[001]	—
5		T_u	$4'/mmm'$	[001]	—
6	T_{2g}	T_{yz}	$4'/mm'm$	[100]	—[a]
7		T_{zx}	$4'/mm'm$	[010]	—[a]
8		T_{xy}	$4'/mm'm$	[001]	—[a]
9	A_{2g}	M_{xyz}	$m\bar{3}m'$	[001]	—
10	T_{1g}	M_x^α	$4/mm'm'$	[100]	σ_{yz}
11		M_y^α	$4/mm'm'$	[010]	σ_{zx}
12		M_z^α	$4/mm'm'$	[001]	σ_{xy}

[a]The multipole magnetic structures characterized by T_{yz}, T_{zx}, and T_{xy} do not induce the AH effect, but those obtained by linear combinations of these MT quadrupoles can induce the AH conductivity in general due to the absence of rotation symmetries.

B. Pyrochlore structure

The pyrochlore crystal structure belongs to the space group $Fd\bar{3}m$ (No. 227), whose crystallographic point group O_h leads to the virtual atomic cluster as shown in Fig. 2(a). The generation procedure of orthonormal magnetic structures gives 12 orthonormal bases characterized by the M dipole and octupole, and the MT quadrupole as shown in Table II. In the pyrochlore structure, the inversion symmetry breaking is accompanied by the breaking of the translation symmetries, since the two atoms related by the space inversion are also transformed by the commensurate translation of the crystal.
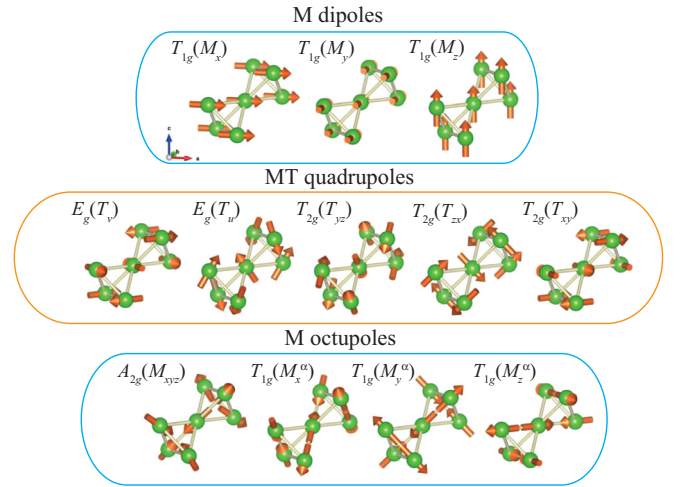

FIG. 5. Multipole magnetic structures in pyrochlore structure characterized by the IREP of O_h point group and its rank. Notations of multipoles are adapted from tables in Ref. [14].

Therefore, a uniform magnetic structure must preserve the space inversion symmetry, restricting the parity-even multipole structures without EM effects. The generated magnetic structure coincides with the basis set obtained in earlier work [28].

The pyrochlore compounds are known to show a variety of magnetic order depending on the atomic constitutions, such as all-in all-out, two-in two-out, and one-in three-out magnetic orders. The relations between the observed magnetic structures and the M multipoles are shown in Table III. The corresponding uniform magnetic orders are shown in Fig. 5. All-in all-out magnetic structures, reported in $Cd_2Os_2O_7$ and $Er_2Ti_2O_7$, correspond to the M_{xyz} octupole in Fig. 5. The magnetic point group of the all-in all-out structure prohibits to induce the AH effect. Meanwhile, the two-in two-out magnetic structure is expressed by a linear combination of the M dipole

TABLE III. Relation between the experimentally observed magnetic structures and the M multipoles in pyrochlore and hexagonal ABO$_3$ crystal structures. $M_{[111]} = (M_x + M_y + M_z)/\sqrt{3}$, and $M_{[111]}^\alpha$ is similarly defined.

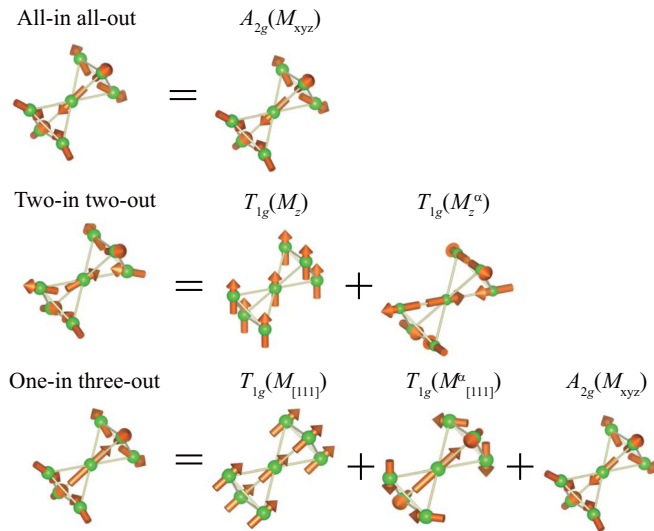| Multipole	IREP	Name	Materials
Pyrochlore			
M_{xyz}	A_{2g}	All-in all-out	$Cd_2Os_2O_7$ [34], $Er_2Ti_2O_7$ [35]
T_{xy}	T_{2g}	—	$Gd_2Sn_2O_7$ [28], $Er_2Ru_2O_7$ [36]
(M_z, M_z^α)	T_{1g}	2-in 2-out	$Ho_2Ru_2O_7$ [37], $Tb_2Sn_2O_7$ [38]
$M_z^\alpha = 2\sqrt{2}M_z$			
(M_z, M_z^α)	T_{1g}	—	$Yb_2Ti_2O_7$ [31], $Yb_2Sn_2O_7$ [32]
M_z dominant			$Tm_2Mn_2O_7$ [33]
$(M_{[111]}, M_{[111]}^\alpha, M_{xyz})$	T_{1g}	1-in 3-out	$Tb_2Ti_2O_7$[a] [39]
Hexagonal ABO$_3$			
M_u	A_2	—	$LuFeO_3$ [40], $ScMnO_3$ (75-129K) [41]
M_{3b}	B_1	—	$HoMnO_3$ (below 40K) [42]
M_{3a}	B_2	—	$HoMnO_3$ (40-75K) [42], $YbMnO_3$ [43]
(M_u, T_z)	$A_2 \oplus A_1$	—	$ScMnO_3$ (below 75K) [41]
(M_{3b}, M_{3a})	$B_1 \oplus B_2$	—	$YMnO_3$ [42]

[a]Stabilized under magnetic fields above 5 T.

FIG. 6. The multipole expansion of all-in all-out, two-in two-out, and one-in three-out magnetic structures in the pyrochlore crystal structure.

and octupole belonging to the T_{1g} IREP as shown in Fig. 6. The two-in two-out magnetic structure is allowed to induce the AH effect by the magnetic point-group symmetry. Since an arbitrary linear combination does not change the symmetry, the pure T_{1g} octupole structure M_z^α without net magnetization can also induce the AH effect. This fact may be relevant to the mechanism of the AH effect of $Pr_2Ir_2O_7$ without net magnetization [29,30]. The order parameter for the magnetic structures of $Yb_2Ti_2O_7$, $Yb_2Sn_2O_7$, and $Tm_2Mn_2O_7$ are also characterized by the T_{1g} multipoles, but in these cases, the M dipole moment is dominant [31–33].

C. Hexagonal ABO$_3$

Hexagonal ABO$_3$ compounds belong to the $P6_3cm$ (No. 185) space group, whose crystallographic point group is C_{6v}, and the corresponding virtual cluster is shown in Fig. 2(d). The magnetic structure generation gives 18 magnetic structures as shown in Fig. 7. The present scheme generates the real basis set, while it contains the complex expressions for two-dimensional IREPs, E_1 and E_2, in the previous work [41]. In Table IV we summarize the relation between the multipole magnetic structures and possible AH and EM effects induced under uniform magnetic order. Table IV shows that the higher-rank multipoles are necessary to fully describe the EM effects.

The magnetic order characterized by the M_u quadrupole is recognized in LuFeO$_3$ and in a temperature range of 75–129 K in ScMnO$_3$ [41]. The M_u quadrupole induces the diagonal components in the EM tensor, $\alpha_{xx} = \alpha_{yy}$ and α_{zz}. The M quadrupole belongs to the A_2 IREP, which is the same as that of the M_z dipole in the C_{6v} crystallographic point group, and hence it can also induce the AH conductivity σ_{xy} as shown in Table III. We note that the M_u quadrupole structure is also regarded as the monopole magnetic structure characterized by M_0, since the same magnetic structure is obtained by using Eq. (12) with the appropriate mapping from the virtual cluster to the crystal unit cell.

The magnetic structures observed in HoMnO$_3$ [42] and YbMnO$_3$ [43] are characterized by M_{3a} and M_{3b} octupoles, which do not induce the EM effect (Table IV). The magnetic structures in YMnO$_3$ and the low-temperature phase in ScMnO$_3$ in Table III are characterized by linear combinations of the multipole structures with different IREPs, which lowers the magnetic point-group symmetry and may lead to additional finite components in the AH conductivity and EM tensors. For instance, the (M_u, T_z) multipole structure of
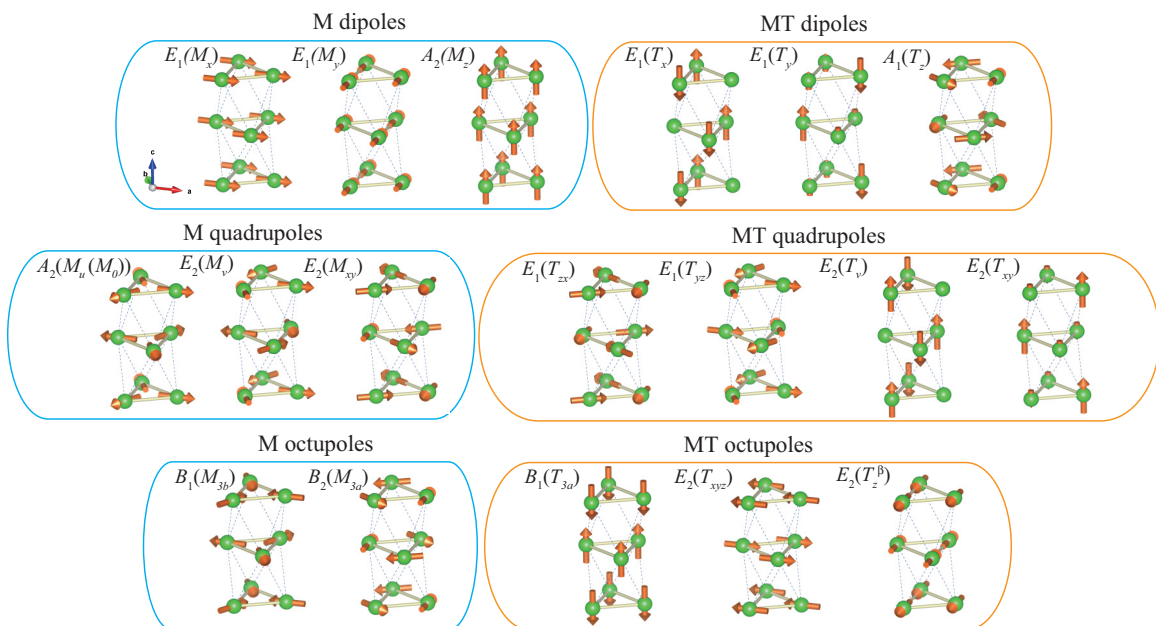

FIG. 7. Multipole magnetic structures in ABO$_3$ characterized by the IREP of the C_{6v} point group and its rank. The notations of multipoles are adapted from tables in Ref. [14].

TABLE IV. Relation between the multipoles corresponding to the orthonormal magnetic structures for hexagonal ABO$_3$ and IREP of C_{6v}, as well as the magnetic point group (MPG) with its principal axis. The active components of the AH conductivity (AHC) and EM tensor are also shown.

No.	IREP	Multipole	MPG	P. axis	AHC	EM
1	E_1	M_x	$mm'2'$	[100]	σ_{yz}	α_{xz}, α_{zx}
2		M_y	$m'm2'$	[100]	σ_{zx}	α_{yz}, α_{zy}
3	A_2	M_z	$6m'm'$	[001]	σ_{xy}	$\alpha_{xx} = \alpha_{yy}, \alpha_{zz}$
4	E_1	T_x	$m'm2'$	[100]	σ_{zx}	α_{yz}, α_{zy}
5		T_y	$mm'2'$	[100]	σ_{yz}	α_{xz}, α_{zx}
6	A_1	T_z	$6mm$	[001]	—	$\alpha_{xy} = -\alpha_{yx}$
7	A_2	M_u	$6m'm'$	[001]	σ_{xy}	$\alpha_{xx} = \alpha_{yy}, \alpha_{zz}$
8	E_2	M_v	$m'm'2$	[100]	σ_{xy}	$\alpha_{xx}, \alpha_{yy}, \alpha_{zz}$
9		M_{xy}	$mm2$	[100]	—	α_{xy}, α_{yx}
10	E_1	T_{yz}	$mm'2'$	[100]	σ_{yz}	α_{xz}, α_{zx}
11		T_{zx}	$m'm2'$	[100]	σ_{zx}	α_{yz}, α_{zy}
12	E_2	T_v	$mm2$	[100]	—	α_{xy}, α_{yx}
13		T_{xy}	$m'm'2$	[100]	σ_{xy}	$\alpha_{xx}, \alpha_{yy}, \alpha_{zz}$
14	B_1	M_{3b}	$6'mm'$	[001]	—	—
15	B_2	M_{3a}	$6'm'm$	[001]	—	—
16	B_1	T_{3a}	$6'mm'$	[001]	—	—
17	E_2	T_{xyz}	$m'm'2$	[100]	σ_{xy}	$\alpha_{xx}, \alpha_{yy}, \alpha_{zz}$
18		T_z^{β}	$mm2$	[100]	—	α_{xy}, α_{yx}

the low-temperature phase of ScMnO$_3$ only preserves sixfold rotation symmetry along the z axis and can have finite σ_{xy} for the AH conductivity [3,6,7] and finite $\alpha_{xx} = \alpha_{yy}$, α_{zz}, and $\alpha_{xy} = -\alpha_{yx}$ for the EM coefficients [2,4]. Meanwhile, the (M_{3b}, M_{3a}) multipole structure of YMnO$_3$ preserves the magnetic point-group symmetry operation of sixfold rotation along the z axis combined with the time-reversal operation, and no AH and EM effects are expected.

IV. SUMMARY

We have proposed a scheme to efficiently generate the symmetry-adapted orthonormal magnetic structures in the crystallographic point group by introducing a virtual atomic cluster to perform the multipole expansion. With this method, we can obtain a magnetic structure that is fully characterized by the M and MT multipole as the suitable order parameters. We have introduced a virtual atomic cluster to obtain the magnetic structures, preserving the magnetic point-group symmetry of the multipoles. We have applied the proposed method to pyrochlore and hexagonal ABO$_3$ crystal structures. For the pyrochlore crystal structure, we have investigated all-in all-out, two-in two-out, and one-in three-out magnetic structures and found that the two-in two-out and one-in three-out magnetic structures are able to be transformed continuously to the pure antiferromagnetic (octupole) structures without net magnetization, leading to the AH effect. For the hexagonal ABO$_3$ crystal structure, the expression of the EM effect is fully identified by the multipole magnetic structures. The proposed scheme paves a way to generate the multipole magnetic structures compatible with the crystallographic point group, which is essential for macroscopic phenomena following Neumann's principle and is useful to search for desired functional magnetic materials.

ACKNOWLEDGMENTS

[1] R. R. Birss, Proc. Phys. Soc. **79**, 946 (1962).

[2] R. R. Birss, *Symmetry and Magnetism* (North-Holland Publishing Company, Amsterdam, 1964).

[3] W. Kleiner, Phys. Rev. **142**, 318 (1966).

[4] J.-P. Rivera, Eur. Phys. J. B **71**, 299 (2009).

[5] D. Szaller, S. Bordács, and I. Kézsmárki, Phys. Rev. B **87**, 014421 (2013).

[6] M. Seemann, D. Ködderitzsch, S. Wimmer, and H. Ebert, Phys. Rev. B **92**, 155138 (2015).

[7] M.-T. Suzuki, T. Koretsune, M. Ochi, and R. Arita, Phys. Rev. B **95**, 094406 (2017).

[8] R. Shindou and N. Nagaosa, Phys. Rev. Lett. **87**, 116801 (2001).

[9] L. Šmejkal, R. González-Hernández, T. Jungwirth, and J. Sinova, arXiv:1901.00445.

[10] C. Ederer and N. A. Spaldin, Phys. Rev. B **76**, 214404 (2007).

[11] N. A. Spaldin, M. Fiebig, and M. Mostovoy, J. Phys.: Condens. Matter **20**, 434203 (2008).

[12] N. A. Spaldin, M. Fechner, E. Bousquet, A. Balatsky, and L. Nordström, Phys. Rev. B **88**, 094429 (2013).

[13] S. Hayami, H. Kusunose, and Y. Motome, Phys. Rev. B **90**, 024432 (2014).

[14] S. Hayami, M. Yatsushiro, Y. Yanagi, and H. Kusunose, Phys. Rev. B **98**, 165110 (2018).

[15] H. Watanabe and Y. Yanase, Phys. Rev. B **98**, 245129 (2018).

[16] T. Higo, H. Man, D. B. Gopman, L. Wu, T. Koretsune, O. M. van' Erve, Y. P. Kabanov, D. Rees, Y. Li, M.-T. Suzuki *et al.*, Nat. Photonics **12**, 73 (2018).

[17] F. Thöle, M. Fechner, and N. A. Spaldin, Phys. Rev. B **93**, 195167 (2016).

[18] S. Nakatsuji, N. Kiyohara, and T. Higo, Nature (London) **527**, 212 (2015).

[19] N. Kiyohara, T. Tomita, and S. Nakatsuji, Phys. Rev. Appl. **5**, 064009 (2016).

[20] A. K. Nayak, J. E. Fischer, Y. Sun, B. Yan, J. Karel, A. C. Komarek, C. Shekhar, N. Kumar, W. Schnelle, J. Kübler *et al.*, Sci. Adv. **2**, e1501870 (2016).

[21] M. Ikhlas, T. Tomita, T. Koretsune, M.-T. Suzuki, D. Nishio-Hamane, R. Arita, Y. Otani, and S. Nakatsuji, Nat. Phys. **13**, 1085 (2017).

[22] J. M. Blatt and V. F. Weisskopf, *Theoretical Nuclear Physics* (Dover Publications, New York, 1991).

[23] H. Kusunose, J. Phys. Soc. Jpn. **77**, 064710 (2008).

[24] D. A. Varshalovich, *Quantum Theory of Angular Momemtum* (World Scientific, Singapore, 1988).

[25] T. Hahn, U. Shmueli, A. J. C. Wilson, and E. Prince, *International Tables for Crystallography* (Kluwer Academic Publishers, Dordrecht, the Netherlands, 2002).

[26] E. F. Bertaut, Acta Crystallographica Section A **24**, 217 (1968).

[27] E. Bertaut, J. Magn. Magn. Mater. **24**, 267 (1981).

[28] A. S. Wills, M. E. Zhitomirsky, B. Canals, J. P. Sanchez, P. Bonville, P. D. d. Réotier, and A. Yaouanc, J. Phys.: Condens. Matter **18**, L37 (2006).

[29] Y. Machida, S. Nakatsuji, S. Onoda, T. Tayama, and T. Sakakibara, Nature (London) **463**, 210 (2010).

[30] S. Nakatsuji, Y. Machida, J. J. Ishikawa, S. Onoda, Y. Karaki, T. Tayama, and T. Sakakibara, J. Phys.: Conf. Ser. **320**, 012056 (2011).

[31] J. Gaudet, K. A. Ross, E. Kermarrec, N. P. Butch, G. Ehlers, H. A. Dabkowska, and B. D. Gaulin, Phys. Rev. B **93**, 064406 (2016).

[32] A. Yaouanc, P. Dalmas de Réotier, P. Bonville, J. A. Hodges, V. Glazkov, L. Keller, V. Sikolenko, M. Bartkowiak, A. Amato, C. Baines *et al.*, Phys. Rev. Lett. **110**, 127207 (2013).

[33] E. Pomjakushina, V. Pomjakushin, K. Rolfs, J. Karpinski, and K. Conder, Inorg. Chem. **54**, 9092 (2015).

[34] J. Yamaura, K. Ohgushi, H. Ohsumi, T. Hasegawa, I. Yamauchi, K. Sugimoto, S. Takeshita, A. Tokuda, M. Takata, M. Udagawa *et al.*, Phys. Rev. Lett. **108**, 247205 (2012).

[35] A. Poole, A. S. Wills, and E. Leliévre-Berna, J. Phys.: Condens. Matter **19**, 452201 (2007).

[36] N. Taira, M. Wakeshima, Y. Hinatsu, A. Tobo, and K. Ohoyama, J. Solid Chem. **176**, 165 (2003).

[37] C. R. Wiebe, J. S. Gardner, S.-J. Kim, G. M. Luke, A. S. Wills, B. D. Gaulin, J. E. Greedan, I. Swainson, Y. Qiu, and C. Y. Jones, Phys. Rev. Lett. **93**, 076403 (2004).

[38] I. Mirebeau, A. Apetrei, J. Rodríguez-Carvajal, P. Bonville, A. Forget, D. Colson, V. Glazkov, J. P. Sanchez, O. Isnard, and E. Suard, Phys. Rev. Lett. **94**, 246402 (2005).

[39] A. P. Sazonov, A. Gukasov, H. B. Cao, P. Bonville, E. Ressouche, C. Decorse, and I. Mirebeau, Phys. Rev. B **88**, 184428 (2013).

[40] S. M. Disseler, J. A. Borchers, C. M. Brooks, J. A. Mundy, J. A. Moyer, D. A. Hillsberry, E. L. Thies, D. A. Tenne, J. Heron, M. E. Holtz *et al.*, Phys. Rev. Lett. **114**, 217602 (2015).

[41] A. Muñoz, J. A. Alonso, M. J. Martínez-Lope, M. T. Casáis, J. L. Martínez, and M. T. Fernández-Díaz, Phys. Rev. B **62**, 9498 (2000).

[42] P. J. Brown and T. Chatterji, J. Phys.: Condens. Matter **18**, 10085 (2006).

[43] X. Fabréges, I. Mirebeau, P. Bonville, S. Petit, G. Lebras-Jasmin, A. Forget, G. Andrè, and S. Pailhès, Phys. Rev. B **78**, 214422 (2008).